Magnetic pumping of whistler waves by tether current modulation

G. Sanchez-Arriaga[1] and J. R. Sanmartin[1]

[1] Magnetic excitation of whistlers by a square array of electrodynamic tethers is discussed. The array is made of perpendicular rows of tethers that carry equal, uniform, and time-modulated currents at equal frequency with a 90° phase shift. The array would fly vertical in the orbital equatorial plane, which is perpendicular to the geomagnetic field $\mathbf{B_0}$ when its tilt is ignored. The array radiates a whistler wave along $\mathbf{B_0}$. A parametric instability due to pumping by the background magnetic field through the radiated wave gives rise to two unstable coupled whistler perturbations. The growth rate is maximum for perturbations with wave vector at angles 38.36° and 75.93° from $\mathbf{B_0}$. For an experiment involving a wavefront that moves with the orbiting array, which might serve to study nonlinear wave interactions and turbulence in space plasmas, characteristic values of growth rate and parameters, such as the number of tethers and their dimensions and distances in the array, are discussed for low Earth orbit ambient conditions.

1. Introduction

[2] This work is a first analysis of a parametric instability to excite whistler waves using electrodynamic tethers in low Earth orbit (LEO). Time-modulated currents carried by the tethers and driven by a power supply result in pumping by the background magnetic field through the radiated wave; coupling in the near field of this wave with whistler perturbations gives rise to the parametric instability. A nonlinear evolution stage, not studied here, may generate a wavefront that could be used to investigate wave-wave interactions and turbulence in space plasmas. Such a large-scale active experiment, with frequency and intensity of a radiated wave controlled and aimed at studying the nonlinear evolution of whistler waves under boundary-free conditions, would hardly be possible on the ground.

[3] Many theoretical works but a limited number of experiments have been carried out on radiation from VLF antennas in space plasmas. Examples are rocket missions by *Barrington* [1969] and *Beghin and Debrie* [1972] and more recently satellites ACTIVNY and IMAGE. These experiments gave insight into a variety of phenomena. In particular, mission ACTIVNY produced effective nonlinear excitation of ion-sound electrostatic turbulence, which converted to lower hybrid resonance noise once radiation ceased [*Molchanov et al.*, 1997]. Whistler and Z mode echoes from radio sounding on the IMAGE satellite were used to provide diagnostics of magnetospheric electron density and irregularities [*Sonwalkar et al.*, 2004].

[4] Orbiting conductors carrying steady currents have been considered for in situ wave emission in the past [*Drell et al.*, 1965; *Barnett and Olbert*, 1986; *Estes*, 1988; *Sanmartin and Martínez-Sánchez*, 1995; *Sanmartin and Estes*, 1997]. The radiation of an electrodynamic tether with time-modulated current has been also studied [*Hastings and Wang*, 1987; *Hastings et al.*, 1988]. The Japan Aerospace Exploration Agency's rocket flight S-520–25 in late August 2009 [*Fuji et al.*, 2009] and National Research Laboratory's CubeSat late this year [*Amatucci et al.*, 2009] are actual space tether missions. Tether array systems, similar to the one proposed here, have been also discussed for electric solar sailing [*Janhunen*, 2004].

[5] The resonant interaction between a pump wave and the natural waves of a continuous system has been extensively studied. A simple general formalism for the coupling of two waves due to the presence of a spatially uniform pump wave was described by *Nishikawa* [1968]; *Liu and Kaw* [1976] reviewed the case for plasmas. Parametric instabilities in inhomogeneous plasmas were originally considered by *Perkins and Flick* [1971], *Rosenbluth* [1972], and *Liu et al.* [1973] and recently by *Afeyan and Williams* [1997], *Short and Simon* [2004], and *Charbonneau-Lefort et al.* [2008].

[6] The parametric excitation of Alfvén waves predicted by *Vahala and Montgomery* [1971], a problem first involving the modulation of a dc magnetic field [*Kaw*, 1976], was observed in the laboratory as early as 1972 [*Lehane and Paoloni*, 1972]. Both Hall and resistivity terms [*Cramer*, 1975] as well as boundary effects [*Cramer and Sy*, 1979] were included in later theoretical analysis. Dusty and multicomponent plasmas have been studied too [*Hertzberg et al.*, 2003; *Hertzberg et al.*, 2004].

[7] This is the first of two papers on the general problem considered, which differ from each other in the tether geom-

etry and the type of waves excited We will here consider a square array of tethers, as has been recently suggested in the (solar) electric sail concept [*Janhunen*, 2004, *Janhunen and Sandroos*, 2007], with the plane of the array perpendicular to the ambient magnetic field and the frequency lying in the classical whistler range having the modulation frequency Ω_1 proportional to the square of the wave vector In a following paper, we will consider a cylindrical array of tethers, with Ω_1 lying in the range below the ion cyclotron frequency

[8] In both cases the tethers would act like an antenna and the required length makes using rigid booms impossible Experimental and theoretical analyses of the near field of a loop antenna operating in the whistler frequency range have found nonuniform plasma structures in the vicinity of the antennas [*Gushchin et al* , 2006, *Korobkov et al* , 2007] Antenna radiation resistance for whistler waves has been recently determined through measurements of whistler wave propagation, formation of propagation ducts was observed [*Amatucci et al* , 2005] Here we have omitted considerations of the near field, and a simple current law will be used We will just require that the driven wave be radiated away from the tether, and we will use the Ampere law as a boundary condition for the magnetic field at the tether surface

[9] The tethers will be assumed at rest in the plasma, as corresponding to LEO orbital velocity $v_{\rm orb} \sim 8$ km/s much less than the Alfven velocity $V_{\rm A}$, which typically lies in the 200–300 km/s range All tethers will be assumed to be of infinite length, which will require that (1) the actual tether length L be large, as advanced, compared to any wavelength in the analysis and (2) this analysis be restricted to a region not too far from the center of the array

[10] This paper is organized as follows In section 2 the magnetic field generated by a square array of tethers carrying a time-modulated current is found The required number of tethers to approximate the square array by a sheet of current is discussed for several frequency domains, the approximation is easiest for whistler waves Starting from the electron-magnetohydrodynamic system, an equation that describes the evolution of the magnetic field is obtained in section 3 The solution is looked for by expanding the magnetic field in three different levels geomagnetic, radiated wave and excited or perturbation waves [*Vahala and Montgomery*, 1971] The wave radiated by the array is found with the boundary condition obtained in section 2 In section 4 the equations describing the perturbations are analyzed, and the growth rate is found in section 5 Possible orbits and characteristic values of some parameters such as mass and power are discussed in section 6 Conclusions are given in section 7

2. A Square Array of Tethers

[11] A tether carrying an active modulated current at a frequency Ω_1 radiates like an antenna In principle, a rigorous determination of the radiated wave requires determining the current in the tether self-consistently with the near-driven fields Here we will just assume a simple current law uniform along the tether

$$I = I_1 \cos \Omega_1 t = \mathrm{Re}[I_1 \exp(-\imath \Omega_1 t)] \tag{1}$$

[12] Note that the case for tethers in a plasma is different, in principle, from the case of a standard antenna, whose current necessarily vanishes at the ends (having negligible capacity), thus being fundamentally nonuniform, tethers can exchange current and present no such restriction In addition, a long enough standard antenna in air presents another source of current non-uniformity, the phase difference for a signal traveling between two points at distance l in the antenna $\Omega_1 \Delta t = \Omega_1\ l/c = k_1 l$ being only ignorable for a tether length $L \ll \lambda_1/2 = \pi/k_1$ A tether in a magnetized plasma, however, behaves differently for whistler and MHD waves, which have large refraction index n, corresponding to negligible displacement current We can then have both $\Omega_1 \Delta t = \Omega_1\ l/c = k_1\ l/n$, say $k_1 L/2n$, small and $k_1 L/2$ large, allowing us to extremely simplify the analysis by keeping I uniform while taking $L \gg \lambda_1$ Ignoring the small displacement current at the low frequency ratio Ω_1/ω_{pe} of interest finally means that sheath charge effects may not have a dominant effect here Actually, the rapid tether-plasma current exchange assumed here might not be technically feasible, tethers carrying uniform, oscillating currents have been studied in the past for radiation impedance considerations [*Hastings and Wang*, 1987, *Hastings et al* , 1988]

[13] The magnetic field generated by an infinitely long tether, centered at the origin and aligned with the z axis, is

$$\mathbf{B} = \frac{\mu_0 I}{2\pi r^2}\,(x\mathbf{u}_{\rm y} - y\mathbf{u}_{\rm x}) \tag{2}$$

[14] For a line array of tethers parallel to the z axis in the $x = 0$ plane and separated by a regular distance Δ, with current I in phase throughout the array, the field is

$$\mathbf{B} = \frac{\mu_0 I}{2\pi} \sum_{s=\ -\infty}^{\infty} \frac{x\mathbf{u}_{\rm y} + (s\Delta - y)\mathbf{u}_{\rm x}}{x^2 + (y - s\Delta)^2} \tag{3}$$

[15] We can approximate this sum as an integral for the distances x of interest, i e , of the order of the wavelength λ_1 for the driven wave

$$\mathbf{B} \approx \frac{\mu_0 I}{2\pi}\left[\int_{\infty}^{\infty} \frac{x\,ds}{x^2 + \Delta^2 s^2}\,\mathbf{u}_{\rm y} + \int_{\infty}^{\infty} \frac{\Delta s\,ds}{x^2 + \Delta^2 s^2}\,\mathbf{u}_{\rm x}\right]$$
$$= \frac{\mu_0 I}{2\Delta}\,\mathrm{sign}(x)\mathbf{u}_{\rm y} \tag{4}$$

if that wavelength is large compared with the distance between tethers

$$\lambda_1 \gg \Delta \tag{5}$$

[16] Equation (4) is the magnetic field created by a sheet of current with surface current density I/Δ, which the field generated by the array rapidly converges to, setting $y = 0$ in equation (3), one readily finds $2B_y\Delta/\mu_0 I = 3\ 4240/\pi$ at $x = 0\ 5\Delta$ and $3\ 1513/\pi$ at $x = \Delta$

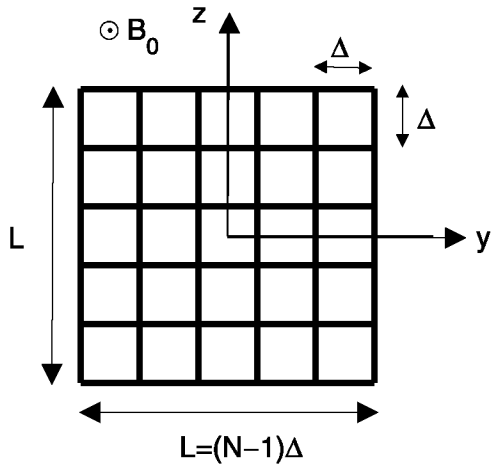

Figure 1. Square array configuration of tethers.

[17] Further, for the simplified analysis of our model to be valid, the array must also be wide as compared with wavelengths:

$$N\Delta \gg \lambda_1. \tag{6}$$

[18] Conditions (5) and (6) may be rewritten in terms of a parameter

$$\varepsilon \equiv \frac{\mu_0 I_1}{2B_0\Delta}, \tag{7}$$

which is the ratio of driven to ambient magnetic fields:

$$1 \ll \frac{\lambda_1}{\Delta} \equiv \varepsilon \frac{4\pi B_0}{\mu_0 I_1 k_1} \ll N. \tag{8}$$

[19] Exciting the fast magnetosonic (FMS) mode of a cold magnetized plasma could typically require too large a number of array tethers in condition (8); using $\Omega_1 \approx V_A k_I$ at frequencies well below the ion cyclotron frequency, we should have, say,

$$N \gg \varepsilon \frac{4\pi m_i V_A}{e\mu_0 I_1} \frac{\Omega_i}{\Omega_1} \approx 2 \times 10^3 \times \frac{\Omega_i}{\Omega_1}, \tag{9}$$

for oxygen ions, $V_A \sim 250$ km/s, $I_1 = 10$ A, and $\varepsilon = 0.05$. The equivalent condition on N for Alfvén waves would just be smaller by the cosine of the angle between $\mathbf{k_1}$ and $\mathbf{B_0}$. Near the frequency Ω_i, this condition replaces the (assumed large) ratio Ω_i/Ω_1 in (9) by the factor $\sqrt{(1 - \Omega_1/\Omega_i)}$, which would require an excitation frequency unreasonably close to Ω_i for sensibly reducing the number of tethers required.

[20] On the other hand, for the whistler range of the FMS mode with Ω_1 well above Ω_i and wave vector $k_1 \propto \sqrt{\Omega_1}$, the ratio Ω_i/Ω_1 in (9) would be replaced by the product $\sqrt{m_e/m_i} \times \sqrt{\Omega_e/\Omega_1}$; a ratio $\Omega_1/\Omega_e \sim 0.1$, say, would allow using a reasonable N value. Considering the array as a sheath of current, the Ampere law immediately gives the magnetic field it generates throughout the $x > 0$ half-space as

$$\varepsilon \mathbf{B}_1(z - \text{line array}) = B_0 \varepsilon \cos(\Omega_1 t)\mathbf{u_y}. \tag{10}$$

[21] Whistlers propagating along an ambient magnetic field are circularly polarized waves rotating around the ambient field direction in the sense of the electron cyclotron motion. To drive a single whistler wave we add a second line array, with tethers parallel to the y axis carrying the same current with a phase shift, $I_1 \sin(\Omega_1 t)$; this generates a field in the $x > 0$ half-space (see Figure 1):

$$\mathbf{B}_1(y - \text{line array}) = B_0 \sin(\Omega_1 t)\mathbf{u_z}. \tag{11}$$

[22] The magnetic field of the full array, written as

$$\mathbf{B}_1(x > 0) = B_0 \mathrm{Re}\left[(\mathbf{u_y} + i\mathbf{u_z}) \exp(-i\Omega_1 t)\right], \tag{12}$$

will be used as a boundary condition on the driven wave in section 3. The length of the tethers will now be $L = (N - 1)\Delta$, which condition (6) shows to be indeed large compared with λ_1. The square array should fly in an equatorial orbit with the geomagnetic field normal when its tilt is ignored (see Figure 2).

3. General Equations and Radiated Wave

[23] Whistlers are described by the equations of the electron magnetohydrodynamics (EMHD) model of a cold plasma, having ion motion ignored,

$$\frac{\partial n_e}{\partial t} + \nabla \cdot (n_e \mathbf{v_e}) = 0 \tag{13}$$

$$\frac{\partial \mathbf{v_e}}{\partial t} + (\mathbf{v_e} \cdot \nabla)\mathbf{v_e} = -\frac{e}{m_e}(\mathbf{E} + \mathbf{v_e} \times \mathbf{B}) - \nu_{ei}\mathbf{v_e} \tag{14}$$

$$\frac{\partial \mathbf{B}}{\partial t} = -\nabla \wedge \mathbf{E} \tag{15}$$

$$\nabla \wedge \mathbf{B} = -e\mu_0 n_e \mathbf{v_e}, \tag{16}$$

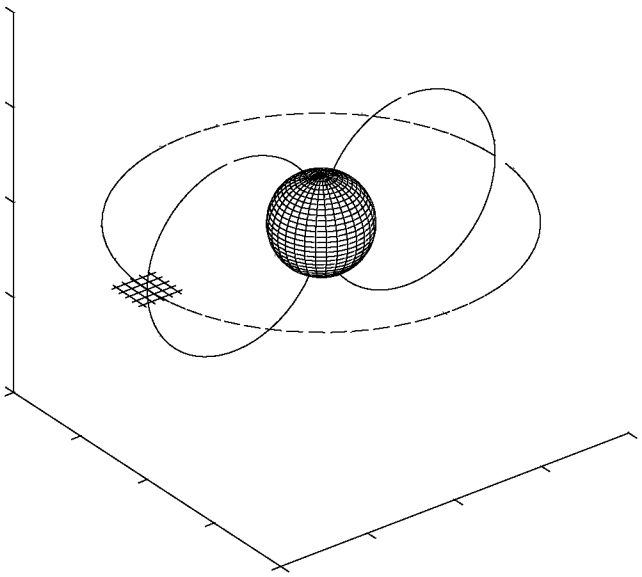

Figure 2. Orbit conditions.

where n_e and $\mathbf{v_e}$ are electron density and velocity, $\mathbf{B}$ and $\mathbf{E}$ are magnetic and electric fields, and ν_{ei} is the frequency of collisions between electrons and ions.

[24] Equations (13) and (16) give $n_e = n_0$. Then, taking the curl of equations (14) and (16) yields

$$\frac{\partial \mathbf{\Omega}}{\partial t} - \nabla \wedge (\mathbf{v_e} \wedge \mathbf{\Omega}) = \frac{\partial \mathbf{\Omega_e}}{\partial t} - \nabla \wedge (\mathbf{v_e} \wedge \mathbf{\Omega_e}) - \nu_{ei}\mathbf{\Omega} \tag{17}$$

$$\mathbf{\Omega} = \frac{c^2}{\omega_{pe}^2}\nabla^2 \mathbf{\Omega_e}, \tag{18}$$

where we defined vectors $\mathbf{\Omega}_e = e\mathbf{B}/m_e$ and (vorticity) $\mathbf{\Omega} = \nabla \wedge \mathbf{v_e}$ and where ω_{pe} and c/ω_{pe} are the electron plasma frequency and skin depth in the ambient plasma, respectively. Considering wave vectors satisfying $k^2 \ll (\omega_{pe}/c)^2$, which corresponds to the classical whistler domain, we have $|\mathbf{\Omega}| \ll |\mathbf{\Omega_e}|$, making the entire LHS of (17) negligible.

[25] Next, using equations (16) and (18) in (17), an equation describing the evolution of the magnetic field is obtained:

$$\frac{\partial \mathbf{b}}{\partial t} - \frac{c^2\Omega_e}{\omega_{pe}^2}\nabla \wedge [\mathbf{b} \wedge (\nabla \wedge \mathbf{b})] - \eta\nabla^2\mathbf{b} = 0, \tag{19}$$

where we wrote $\mathbf{B} = B_0\mathbf{b}$ and $\eta \equiv \nu_{ei}c^2/\omega_{pe}^2$, which is a diffusivity. Equation (19) must here be solved in the half-space $x > 0$ following the scheme introduced by *Vahala and Montgomery* [1971]. The magnetic field is made of three contributions of disparate magnitude:

$$\mathbf{b} = \mathbf{b}_0 + \varepsilon\mathbf{b}_1 + \mathbf{b}^1. \tag{20}$$

[26] The field $\mathbf{b}_0$ refers to the geomagnetic field directed along $\mathbf{u_x}$ (see Figures 1 and 2), $\mathbf{b_1}$ is the radiated wave and $\mathbf{b^1}$ the perturbations or excited waves. The scaling $\mathbf{b_0} \gg \varepsilon\mathbf{b_1} \gg \mathbf{b^1}$ is assumed. The boundary condition at $x = 0^+$ is obtained from equations (12) and (20):

$$\mathbf{b}(x = 0^+) = \mathrm{Re}\left[\mathbf{u_x} + \varepsilon(\mathbf{u_y} + i\mathbf{u_z})e^{-i\Omega_1 t}\right]. \tag{21}$$

[27] To keep the development compact, we will use complex notation for the fields.

[28] The radiated wave is obtained by substituting equation (20) in equation (19) and collecting terms of order ε. Using $\nabla \cdot \mathbf{u_x} = 0$ and $\nabla \cdot (\nabla \wedge \mathbf{b_1}) = 0$, we find

$$\frac{\partial \mathbf{b_1}}{\partial t} - \eta\nabla^2\mathbf{b_1} + \frac{\Omega_e c^2}{\omega_{pe}^2}\frac{\partial}{\partial x}(\nabla \wedge \mathbf{b_1}) = 0. \tag{22}$$

[29] The solution to equation (22) satisfying boundary condition (21) takes the form

$$\mathbf{b_1} = \boldsymbol{\beta}\, e^{i(k_1 x - \Omega_1 t)} + cc \tag{23}$$

$$\boldsymbol{\beta} \equiv \frac{\mathbf{u_y} + i\mathbf{u_z}}{2}, \tag{24}$$

with cc denoting complex conjugated. Using $\nabla \wedge \mathbf{b_1} \equiv k_1\mathbf{b_1}$ and defining $\alpha = \omega_{pe}^2/c^2\Omega_e$, (22) becomes

$$\frac{\partial \mathbf{b_1}}{\partial t} - \eta\frac{\partial^2 \mathbf{b_1}}{\partial x^2} + \frac{k_1}{\alpha}\frac{\partial \mathbf{b_1}}{\partial x} = 0, \tag{25}$$

yielding the dispersion relation for whistlers

$$k_1 = \pm\sqrt{\alpha\Omega_1}\left(1 + \frac{i}{2}\frac{\nu_{ei}}{\Omega_e}\right), \tag{26a}$$

$$\Omega_1 = \Omega_e\frac{c^2k_1^2}{\omega_{pe}^2}\left(1 - i\frac{\nu_{ei}}{\Omega_e}\right), \tag{26b}$$

where a weak collision frequency, $\nu_{ei} \ll \Omega_e$, was assumed. The physical solution to (25) corresponds to the plus sign in equation (26a), showing waves to decay as $x \to +\infty$.

4. Excited Waves

[30] Perturbations to the background made of ambient plasma and driven fields are studied collecting terms linear in $\mathbf{b^1}$ and $\varepsilon\mathbf{b^1}$ in equation (19):

$$\alpha\left(\frac{\partial}{\partial t} - \eta\nabla^2\right)\mathbf{b^1} = \nabla \wedge \left[(\mathbf{u_x} + \varepsilon\mathbf{b_1}) \wedge (\nabla \wedge \mathbf{b^1})\right] + \nabla \wedge \left[\mathbf{b^1} \wedge (\nabla \wedge \varepsilon\mathbf{b_1})\right]. \tag{27}$$

[31] Using again $\nabla \wedge \mathbf{b_1} = k_1\mathbf{b_1}$, and $\nabla \cdot \mathbf{b} = 0$, equation (27) reads

$$\alpha\left(\frac{\partial}{\partial t} - \eta\nabla^2\right)\mathbf{b^1} + \frac{\partial}{\partial x}(\nabla \wedge \mathbf{b^1}) = \varepsilon\left[(\nabla \wedge \mathbf{b^1} - k_1\mathbf{b^1}) \cdot \nabla\mathbf{b_1} - \mathbf{b_1} \cdot \nabla(\nabla \wedge \mathbf{b^1} - k_1\mathbf{b^1})\right]. \tag{28}$$

[32] No general solution to equation (28) can be given because of coefficients variable in time and space due to the driven fields. Determining growth rates is possible, however, for perturbations only composed of two waves linked by a resonance condition and ignoring off-resonance terms.

[33] To handle products of terms with subscript 1 (driven fields) and superscript 1 (perturbations) in equation (28), we keep the complex notation for the real fields:

$$\mathbf{b^1} = \mathbf{b_a}e^{i(\mathbf{k_a}\,\mathbf{r} - \omega_a t)} + \mathbf{b_b}e^{i(\mathbf{k_b}\,\mathbf{r} - \omega_b t)} + \mathrm{cc}. \tag{29}$$

[34] Consider waves with subscripts a and b satisfying the resonance conditions:

$$\mathrm{Re}(\omega_a + \omega_b) = \Omega_1 \tag{30a}$$

$$\mathrm{Im}(\omega_a - \omega_b) = 0 \tag{30b}$$

$$k_{xa} + k_{xb} = k_1 \tag{31a}$$

$$\mathbf{k}_{\perp a} + \mathbf{k}_{\perp b} = 0. \tag{31b}$$

[35] Using (23) and (29) in equation (28), $\mathbf{b_a}$ terms proportional to $e^{\imath(\mathbf{k_a}\,\mathbf{r}-\omega_a t)}$ on the LHS are coupled to both the $\mathbf{b^*_b}$ term and the first term of (23) on the RHS so as to yield identical space and time dependence on both sides of (28):

$$k_{ax}\mathbf{k_a}\wedge\mathbf{b_a}+\alpha(\imath\omega_a-\eta k_a^2)\mathbf{b_a}=\varepsilon\Big[k_1\boldsymbol{\beta}\otimes\mathbf{u_x}\quad\Big(\imath k_1\mathbf{b}_\mathbf{b}^*-\mathbf{k_b}\wedge\mathbf{b}_\mathbf{b}^*\Big)+\boldsymbol{\beta}\quad\mathbf{k_b}\Big(\imath k_1\mathbf{b}_\mathbf{b}^*-\mathbf{k_b}\wedge\mathbf{b}_\mathbf{b}^*\Big)\Big] \tag{32}$$

[36] Equation (32) and the corresponding equation for $\mathbf{b^*}_b$ constitute a homogeneous system with six unknown variables, the compatibility condition yielding a dispersion relation. Writing $\mathbf{k}\wedge\mathbf{b}\equiv\bar{\bar{k}}\cdot\mathbf{b}$ where $\bar{\bar{k}}$ is the tensor

$$\bar{\bar{k}}\equiv\begin{pmatrix}0&-k_z&k_y\\k_z&0&-k_x\\-k_y&k_x&0\end{pmatrix}, \tag{33}$$

equation (32) becomes, in a matrix form,

$$\bar{\bar{M}}_a\mathbf{b_a}=\bar{\bar{N}}_b^*\mathbf{b}_\mathbf{b}^*, \tag{34}$$

with

$$\bar{\bar{M}}_a\equiv k_{xa}\bar{\bar{k}}_a+\alpha(\imath\omega_a-\eta k_a^2)\bar{\bar{U}} \tag{35}$$

$$\bar{\bar{N}}_b^*\equiv\varepsilon\Big[k_1\boldsymbol{\beta}\otimes\mathbf{u_x}+(\mathbf{k_b}\quad\boldsymbol{\beta})\bar{\bar{U}}\Big]\quad\Big(\imath k_1\bar{\bar{U}}-\bar{\bar{k}}_b\Big), \tag{36}$$

where $\bar{\bar{U}}$ is the unitary matrix. From (34), we can immediately write

$$\bar{\bar{M}}_b^*\mathbf{b}_\mathbf{b}^*=\bar{\bar{N}}_a\mathbf{b_a} \tag{37}$$

[37] Next, with equations (34) and (37), one readily obtains

$$\Big(\bar{\bar{U}}-\bar{\bar{M}}_a^{-1}\bar{\bar{N}}_b^*\Big(\bar{\bar{M}}_b^{-1}\Big)^*\bar{\bar{N}}_a\Big)\mathbf{b_a}=0 \tag{38}$$

[38] Since the problem has axial symmetry around $\mathbf{u_x}$, we can set $k_z=0$ and write

$$k_{ya}=-k_{yb}\equiv k_y$$

with no loss of generality. Then, matrices are given as

$$\bar{\bar{M}}(\omega,\mathbf{k})=k_x\bar{\bar{k}}+\alpha(\imath\omega-\eta k^2)\bar{\bar{U}}=\begin{pmatrix}\alpha(\imath\omega-\eta k^2)&0&k_xk_y\\0&\alpha(\imath\omega-\eta k^2)&-k_x^2\\-k_xk_y&k_x^2&\alpha(\imath\omega-\eta k^2)\end{pmatrix} \tag{39}$$

$$\bar{\bar{N}}^*(\mathbf{k})=\varepsilon\Big(k_1\boldsymbol{\beta}\otimes\mathbf{u_x}+(\mathbf{k}\quad\boldsymbol{\beta})\bar{\bar{U}}\Big)\quad\Big(\imath k_1\bar{\bar{U}}-\bar{\bar{k}}\Big)=\frac{\varepsilon}{2}\begin{pmatrix}\imath k_1k_y&0&-k_y^2\\\imath k_1^2&\imath k_1k_y&(k_x-k_1)k_y\\k_y^2-k_1^2&-k_xk_y&0\end{pmatrix}, \tag{40}$$

where, writing $\mathbf{k_a}$, ω_a ($\mathbf{k_b}$, ω_b) for $\mathbf{k}$, ω would yield $\bar{\bar{M}}_a$, $\bar{\bar{N}}_a$ ($\bar{\bar{M}}_b$, $\bar{\bar{N}}_b$). The inverse of $\bar{\bar{M}}$ reads

$$\bar{\bar{M}}^{-1}(\omega,\mathbf{k})=\frac{\bar{\bar{L}}(\omega,\mathbf{k})}{D(\omega,\mathbf{k})}, \tag{41}$$

where

$$\bar{\bar{L}}(\omega,\mathbf{k})\equiv\frac{\imath}{\alpha\omega}\begin{pmatrix}k_x^4-\alpha^2\omega^2&k_x^3k_y&-\imath\alpha\omega k_xk_y\\k_x^3k_y&k_x^2k_y^2-\alpha^2\omega^2&\imath\alpha\omega k_x^2\\\imath\alpha\omega k_xk_y&-\imath\alpha\omega k_x^2&-\alpha^2\omega^2\end{pmatrix}, \tag{42}$$

$$D(\omega,\mathbf{k})\equiv\alpha^2\big(\omega^2+2\imath\omega\eta k^2\big)-k_x^2k^2 \tag{43}$$

[39] Damping is assumed small and terms involving the product between ε and η are neglected; the resistivity contribution was ignored in the auxiliary matrix $\bar{\bar{L}}$ while kept in $D(\omega,\mathbf{k})$ for use in the dispersion relation.

5. Dispersion Relation

[40] The dispersion relation for $\varepsilon=0$ and $\eta=0$, reading $D(\omega,\mathbf{k})=0$ or $\alpha\omega|_{\varepsilon=0}=k_xk$, for either mode a or b as a whistler wave, will be only slightly modified by the driven fields. We may use $\varepsilon=0$ frequency values in just the matrix $\bar{\bar{L}}$, which takes an extremely simple form as the dyadic product of a vector:

$$\mathbf{c}=\begin{pmatrix}k_y,&-k_x,&-\imath k\end{pmatrix} \tag{44}$$

and its complex conjugate

$$\bar{\bar{L}}(\mathbf{k})=-\imath\frac{k_x}{k}\mathbf{c}\otimes\mathbf{c}^* \tag{45}$$

[41] The dispersion relation then reads

$$\Big|D(\omega_a,\mathbf{k_a})D^*\Big(\omega_b^*,\mathbf{k_b}\Big)\bar{\bar{U}}-\frac{k_{xa}k_{xb}}{k_ak_b}\mathbf{c_a}\otimes\mathbf{c}_\mathbf{a}^*\bar{\bar{N}}_b^*\mathbf{c}_\mathbf{b}^*\otimes\mathbf{c_b}\bar{\bar{N}}_a\Big|=0 \tag{46}$$

[42] To determine the small ε corrections taking into account the resonance conditions (30) and (31) and setting $\mathrm{Re}(\omega_a+\omega_b)|_{\varepsilon=0}=\Omega_1$, or $k_{xa}k_a+k_{xb}k_b=k_1^2$, the frequencies are written as

$$\omega_a=\frac{k_{xa}k_a}{\alpha}+\Omega_1(\varphi+\imath\tilde{\gamma}) \tag{47a}$$

$$\omega_b^*=\frac{k_{xb}k_b}{\alpha}-\Omega_1(\varphi+\imath\tilde{\gamma}), \tag{47b}$$

where φ and $\tilde{\gamma}$ are the dimensionless frequency shift and growth rate, respectively. The dispersion relation becomes (see section A)

$$\Big[(\varphi+\imath\tilde{\gamma})^2+\frac{\imath\eta}{\Omega_1}(\varphi+\imath\tilde{\gamma})\big(k_a^2+k_b^2\big)\Big]=\varepsilon^2J, \tag{48}$$

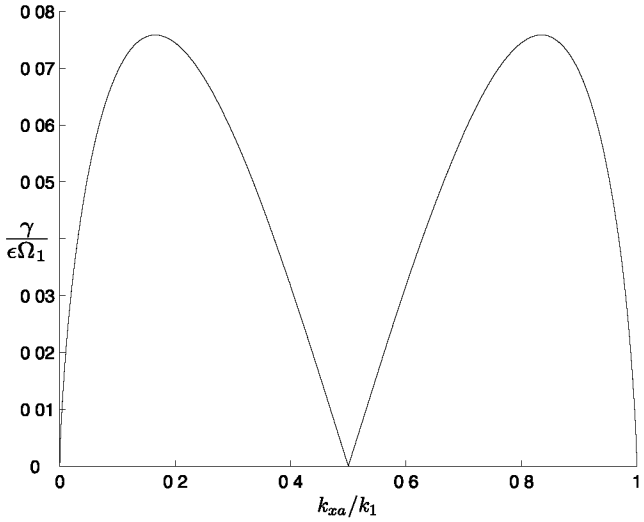

Figure 3. Normalized growth rate versus k_{xa}/k_1 at $\eta = 0$

where

$$J = \frac{k_y^2[(k_1 - k_a - k_b)k_a + 2k_1k_{xa}][(k_1 - k_a - k_b)k_b + 2k_1k_{xb}]}{16k_1^4k_ak_b} \tag{49}$$

[43] Taking the ansatz $J < 0$, the solution to equation (48) reads

$$\varphi + \imath\tilde{\gamma} = -\imath\frac{\eta(k_a^2 + k_b^2)}{2\Omega_1} \pm \imath\sqrt{\varepsilon^2|J| + \left[\frac{\eta(k_a^2 + k_b^2)}{2\Omega_1}\right]^2} \tag{50}$$

[44] It clearly follows that first $\varphi \equiv 0$ and second there is a positive $\tilde{\gamma}$ root (growth rate) whenever $|J| > 0$ There is thus no threshold on the instability

[45] From the resonance conditions (31a) and $k_{xa}k_a + k_{xb}k_b = k_1^2$, there follows a relation

$$F(\kappa_a, \kappa_b) \equiv \kappa_a\sqrt{1 + \kappa_a^2} + \kappa_b\sqrt{1 + \kappa_b^2} - (\kappa_a + \kappa_b)^2 = 0 \tag{51}$$

between $\kappa_a \equiv k_{xa}/k_y$ and $\kappa_b \equiv k_{xb}/k_y$ A fixed point $F(\kappa^*, \kappa^*) = 0$ occurs at $\kappa_a = \kappa_b = \kappa^* \equiv 1/\sqrt{3}$ Further, from equation (49) we can also obtain a function G of κ_a and κ_b to allow writing $J \equiv CG(\kappa_a, \kappa_b)G(\kappa_b, \kappa_a)$, with C being a positive factor, one then readily verifies the vanishing of G at the fixed point of F Finally, writing $\kappa_a = \kappa^* + \Delta\kappa_a$, $\kappa_b = \kappa^* + \Delta\kappa_b$ with $\Delta\kappa_a$ and $\Delta\kappa_b$ small, in equation (51) we find $\Delta\kappa_a = -\Delta\kappa_b$, whereas J takes the form

$$J = C\left[\left(\frac{\partial}{\partial\kappa_a} - \frac{\partial}{\partial\kappa_b}\right)G(\kappa_a, \kappa_b)\Big|_{\kappa^*\,\kappa^*}\right]^2 \Delta\kappa_a\Delta\kappa_b \tag{52}$$

proving J negative at some κ_a range around κ^*

[46] Figure 3 shows the (positive) rate $\gamma \equiv \Omega_1\tilde{\gamma}$ versus the normalized wave vector component k_{xa}/k_1 when $\eta = 0$ proving the ansatz The maximum growth rate, attained at $k_{xa}/k_1 \approx 0\ 17$ and $k_{xa}/k_1 \approx 0\ 83$, is $\tilde{\gamma}_{\max}/\varepsilon \approx 0\ 0758$ At $k_{xa}/k_1 = 0\ 5$, corresponding to $\kappa_a = \kappa_b = \kappa^*$, the growth rate vanishes as previously noticed

[47] Figure 4 is a polar diagram of the dimensionless growth rate $\tilde{\gamma}/\varepsilon$ as a function of the angle θ_a between the wave vector $\mathbf{k_a}$ and the x axis, with $\cos\theta_a \equiv k_{xa}/k_a$ when $\eta = 0$ There are two lobes corresponding to the two maxima in Figure 3, which occur at $\theta_a \approx 38\ 36°$ and $\theta_a \approx 75\ 93°$ The parametric instability describes early dynamics, with the evolution of the nonlinear wavefront definitely more complicated However, a footprint of the two lobes might possibly be present in the nonlinear stage and it could be measured in an experiment

[48] The parametric instability analysis showed that for each wave with angle θ_a, there is a second wave with θ_b and the same growth rate Note that both rate maxima are equal, in agreement with the waves at $38\ 36°$ and $75\ 93°$ being coupled to each other Waves propagating at different inclinations to the array behave differently, however, making the shape of the two lobes different

6. Discussion

[49] The choice of the orbit is determined by a set of requirements involving plasma ambient conditions, the properties of the excited wavefront, and technological considerations (mass and power) An equatorial circular orbit, with the planar array flying vertical (see Figures 1 and 2), would be an appropriate choice because the geomagnetic field would be always normal to the array and the gravity gradient could be used for stability considerations [*Arnold*, 1987] On the other hand, the wavelength λ_1 determines the length of the tethers and it has a direct impact on the mass and the required power As we will see, a low altitude orbit reduces the mass requirements because the wavelength of the radiated wave decreases with the plasma density as $\lambda_1 \sim n_0^{1/2}$ A low Earth orbit would then appear to be the best choice

[50] The system mass would be basically made of tether hardware and power subsystem

$$M_S = M_{\text{arr}} + \alpha\dot{W}_{\text{Ohm}} = 2NL\left(\rho A_{cs} + \frac{\alpha I_1^2}{\sigma_c A_{cs}}\right), \tag{53}$$

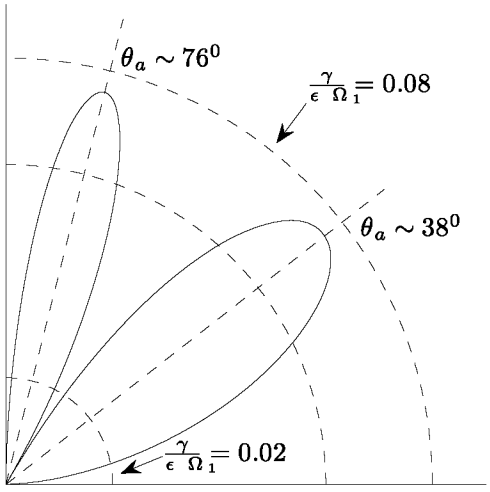

Figure 4. Polar diagram for the dimensionless growth rate at $\eta = 0$

Table 1. Characteristic Values for $A_{cs} = 2$ mm^2, $\delta = 5$, $N = 100$, $B_0 = 0.3$ G, $n_0 = 10^6$/cm^3, and $\eta = 0$

Ω_1/Ω_e	λ_1 (m)	L (m)	Δ (m)	ε	γ_{max} (kHz)	$\dot{W}_{Ohm}$ (kW)	M_S (kg)
0 1	100	500	5 1	0 018	0 72	27	1090
0 3	51	255	2 6	0 036	4 25	13	555

where the Ohmic power was assumed to be dominant, α is the inverse specific power of the power supply and ρ and σ_c are the tethers' density and conductivity, respectively. A minimum of total mass is reached at

$$A_{cs} = I_1 \sqrt{\frac{\alpha}{\sigma_c \rho}} \tag{54}$$

and the minimum mass is

$$M_S|_{\min} = 4NLI_1 \sqrt{\frac{\alpha\rho}{\sigma_c}} = \frac{8\varepsilon B_0 L^2}{\mu_0} \frac{N}{N-1} \sqrt{\frac{\alpha\rho}{\sigma_c}}, \tag{55}$$

where we used equation (7) and $L = (N-1)\Delta$. The length of the tethers is now written in terms of the wavelength $L \equiv \delta\lambda_1$, where δ is a large enough dimensionless number that makes the infinite length hypothesis valid. The wavelength λ_1 is related to the driven frequency Ω_1 by the dispersion relation (26a) that assumes $\Omega_1 \ll \Omega_e$. In the general case the wavelength is given by the whistler dispersion relation

$$\frac{\Omega_1}{\Omega_e} = \frac{c^2 k_1^2/\omega_{pe}^2}{1 + c^2 k_1^2/\omega_{pe}^2} \tag{56a}$$

or

$$\lambda_1 = \frac{2\pi c}{\omega_{pe}} \sqrt{\frac{1 - \Omega_1/\Omega_e}{\Omega_1/\Omega_e}}. \tag{56b}$$

[51] Substituting $L \equiv \delta\lambda_1$ and equation (56) in (55) yields

$$M_S|_{\min}\left(\varepsilon, \frac{\Omega_1}{\Omega_e}, \delta\right) = K \frac{1 - \Omega_1/\Omega_e}{\Omega_1/\Omega_e} \varepsilon\delta^2, \tag{57}$$

where K is a factor that depends on the orbit and the characteristic of the tether:

$$K \equiv \frac{32\pi^2 B_0 m_e}{\mu_0^2 n_0 e^2} \frac{N}{N-1} \sqrt{\frac{\alpha\rho}{\sigma_c}} \approx \frac{32\pi^2 B_0 m_e}{\mu_0^2 n_0 e^2} \sqrt{\frac{\alpha\rho}{\sigma_c}}. \tag{58}$$

[52] Equation (57) is a valid expression for an experiment to excite whistler waves using a square array of tethers. Note, however, that the growth rate obtained in section 5 requires (i) $\varepsilon \ll 1$ for keeping our perturbation method valid, (ii) $\Omega_1/\Omega_e \ll 1$ for neglecting the LHS of equation (17), and (iii) $\delta \gg 1$ for ignoring array edge effects. Typical LEO ambient values ($B_0 \approx 0.3G$, $n_0 = 10^6$/cm^3), tether parameters ($\rho = 2.7 \times 10^3$ kg/m^{-3}, $\sigma_c = 3.5 \times 10^7$/ohm^1/m^1) and an inverse specific power $\alpha = 20$ kg/kW [*Stark*, 2003], yield $K = 265$ kg. Equation (58) shows that high plasma density and better technological coefficient (α, ρ, and σ_c) decrease the mass of the system.

[53] The growth rate, which governs the characteristic time for the development of the wavefront, depends on the electron gyrofrequency and the resistivity too. In LEO one finds $\Omega_e \approx 5.2 \times 10^6$ rad/s and the collision frequency between electrons and ions:

$$\nu_{et}(s^{-1}) = 2.9 \times 10^{-12} \frac{n_e(m^{-3}) \ln(\Lambda)}{T_e(\text{eV})^{3/2}}. \tag{59}$$

[54] Assuming $\ln \Lambda \approx 15$ and $T_e = 0.1$ eV yields $\nu_{et} = 1.4 \times 10^3$ s^{-1}, which produces a very small correction for the growth rate in equation (50): $\eta(k_a^2 + k_b^2)/2\Omega_1 \approx \eta k_1^2/\Omega_1 = \nu_{et}/\Omega_e \approx 0.0016$. The typical space scale to damp out the driven fields is very large too (see equation (26)) $\text{Im}(\lambda_1) \approx 250 \times \sqrt{\Omega_e/\Omega_1}$ km.

[55] For a round tether of radius $R = 0.8$ mm ($A_{cs} = 2$ mm^2), the intensity that minimizes the mass is from equation (54): $I_1 = 4.37$ A. Table 1 summarizes the characteristic parameters of the experiment assuming the previous values and $\delta = 5$, $N = 100$, and $\eta = 0$. Two modulation frequencies, $\Omega_1/\Omega_e = 0.1$ and $\Omega_1/\Omega_e = 0.3$, are considered. In the latter case the LHS of equation (17) should be retained. Higher modulation frequency not only increases the growth rate, but also decreases the total mass.

[56] Consideration of mass, power, and structural forces in the array system would be relevant for design purposes. The Lorentz force LI_1B_0 of the geomagnetic field on any tether in the array, which rapidly oscillates at frequency Ω_1, will vanish on the average. Similarly, the force between perpendicular array tethers, which varies as $\sin 2\Omega_1 t$, will vanish when averaged too. Forces between parallel tethers will have nonzero average, however. Tethers at the end of a line will experience the largest Lorentz force:

$$F_1 = \frac{\mu_0 L I_1^2}{2\pi\Delta}\left(1 + \frac{1}{2} + \frac{1}{3} + \quad + \frac{1}{N-1}\right) \approx \frac{\varepsilon}{\pi}\left[0.577 + \ln N - \frac{1}{2N}\right] LB_0 I_1. \tag{60}$$

7. Conclusions

[57] Use of electrodynamic tethers for space applications other than propulsion or power generation have been discussed recently; these include, in particular, radiation belt remediation [*Inan et al.*, 2003], solar electric sailing [*Janhunen*, 2004; *Janhunen and Sandroos*, 2007] and generation of electron beams for the production of artificial auroras [*Sanmartin et al.*, 2006]. In this work we considered an application of scientific interest, involving the parametric excitation of whistler waves by a square array of electrodynamic tethers to produce and study nonlinear wave interactions and turbulence in space plasmas.

[58] The array would lie in the vertical, equatorial orbital plane. With its tilt neglected, the geomagnetic field would be perpendicular to the orbital plane and array. One line of tethers will be aligned vertically and regularly spaced, each tether carrying a current uniform along its length and time modulated with frequency Ω_1; to radiate one whistler wave, a second line array of tethers will lie horizontal with the current phase shifted by 90°.

[59] The maximum growth of coupled whistler perturbations is found to occur at angles of 38.36° and 75.93° from the geomagnetic field. Characteristic values of growth rate and parameters such as the number of tethers, and their dimensions and distance in the array, have been determined for the ambient conditions at an experiment involving the whistler wavefront that moves with the array in a low Earth orbit.

Appendix A: Analytical Derivation of the Growth Rate

[60] Taking into account equations (47a) and (47b), both $D(\omega_a, \mathbf{k_a})$ and $D^*(\omega^*_b, \mathbf{k_b})$ can be approximated as

$$D(\omega_a, \mathbf{k_a}) = \alpha^2\left(\omega_a^2 + 2\imath\omega_a\eta k_a^2\right) - k_{xa}^2 k_a^2 \approx 2\alpha k_{xa} k_a\left[\Omega_1(\varphi + \imath\tilde{\gamma}) + \imath\eta k_a^2\right], \tag{A1}$$

$$D^*\left(\omega_b^*, \mathbf{k_b}\right) = \alpha^2\left(\omega_b^{*2} - 2\imath\omega_b^*\eta k_b^2\right) - k_{xb}^2 k_b^2 \approx -2\alpha k_{xb} k_b\left[\Omega_1(\varphi + \imath\tilde{\gamma}) + \imath\eta k_b^2\right] \tag{A2}$$

[61] The dispersion relation then reads

$$\left|\left[(\varphi + \imath\tilde{\gamma})^2 + \frac{\imath\eta}{\Omega_1}(\varphi + \imath\tilde{\gamma})\left(k_a^2 + k_b^2\right)\right]\overline{\overline{U}} - \varepsilon^2\overline{\overline{J}}\right| = 0, \tag{A3}$$

where

$$\overline{\overline{J}} = -\frac{\mathbf{c_a^*}\overline{\overline{N}}_b^*\mathbf{c_b^*}}{\left(2\varepsilon^2 k_1^2 k_a k_b\right)^2}\mathbf{c_a} \otimes \mathbf{c_b}\overline{\overline{N}}_a \tag{A4}$$

[62] Matrix $\overline{\overline{J}}$ is then written as the tensorial product of two vectors $\mathbf{c_a}$ and $\mathbf{c_b}\overline{\overline{N}}_a$. Using the identity

$$\left|\mu\overline{\overline{U}} - \mathbf{u} \otimes \mathbf{v}\right| = \mu^2[\mu - tr(\mathbf{u} \otimes \mathbf{v})] \tag{A5}$$

allows us to write equation (A3) as

$$\left[(\varphi + \imath\tilde{\gamma})^2 + \frac{\imath\eta}{\Omega_1}(\varphi + \imath\tilde{\gamma})\left(k_a^2 + k_b^2\right)\right] = \varepsilon^2 tr\left(\overline{\overline{J}}\right) \equiv \varepsilon^2 J \tag{A6}$$

[63] The trace J is found with the following steps. First, the numerator in (A4) is obtained:

$$\mathbf{c_a^*}\overline{\overline{N}}_b^* = \frac{\imath\varepsilon}{2}\left(k_y^2(k_a - k_1) - k_1^2(k_{xa} + k_a),\ k_y(k_a k_{xb} + k_1 k_{xa}),\ \imath k_y k_a^2\right) \tag{A7}$$

$$\mathbf{c_a^*}\overline{\overline{N}}_b^*\mathbf{c_b^*} = \frac{\imath\varepsilon}{2}k_a k_y[k_a(k_1 - k_a - k_b) + 2k_1 k_{xa}] \tag{A8}$$

[64] On the second place, the vector $\mathbf{c_b}\overline{\overline{N}}_a$ is

$$\mathbf{c_b}\overline{\overline{N}}_a = -\frac{\imath\varepsilon}{2}\left(k_y^2(k_b - k_1) - k_1^2(k_{xb} + k_b),\ -k_y(k_b k_{xa} + k_1 k_{xb}),\ \imath k_y k_b^2\right) \tag{A9}$$

[65] Note that it is not necessary to compute the whole matrix $\vec{c}_a \otimes \vec{c}_b\overline{\overline{N}}_a$, and just the trace is given by

$$tr\left(\mathbf{c_a} \otimes \mathbf{c_b}\overline{\overline{N}}_a\right) = \frac{\imath\varepsilon}{2}k_b k_y[k_b(k_1 - k_a - k_b) + 2k_1 k_{xb}] \tag{A10}$$

[66] Using equations (A4), (A8) and (A10) finally yields

$$J = \frac{k_y^2[(k_1 - k_a - k_b)k_a + 2k_1 k_{xa}][(k_1 - k_a - k_b)k_b + 2k_1 k_{xb}]}{16k_1^4 k_a k_b} \tag{A11}$$

[67] **Acknowledgments.** This work was supported by the Ministry of Science and Technology of Spain under grant no ESP2004-01511

[68] Amitava Bhattacharjee thanks Bedros Afeyan and another reviewer for their assistance in evaluating this paper

References

Afeyan, B B , and E A Williams (1997), A variational approach to parametric instabilities in inhomogeneous plasmas I Two model problems, *Phys Plasmas*, *4*(11), 3788–3802, doi 10 1063/1 872504

Amatucci, W E , D D Blackwell, D N Walker, G Gatling, and G Ganguli (2005), Whistler wave propagation and whistler wave antenna radiation resistance measurements, *IEEE Trans Plasma Sci* , *33*, 637–646, doi 10 1109/TPS 2005 844607

Amatucci, B , S Arnold, S Coffey, G Gatling, S Huynh, P Jaffe, B Kelm, S Koss, J McGahagan, and A Thurn (2009), CE2 A CubeSat electron collector experiment, paper AAS 09-239 presented at 19th Space Flight Mechanics Meeting, Am Astronaut Soc , Savannah, Ga

Arnold, D A (1987), The behavior of long tethers in space, *J Astronaut Sci* , *35*(1), 3–18

Barnett, A , and S Olbert (1986), Radiation of plasma waves by a conducting body moving through magnetized plasma, *J Geophys Res* , *91*, 10,117–10,135

Barrington, R E (1969), *Plasma Waves in Space and in the Laboratory*, vol 1, 361 pp , Edinburg Univ Press, Edinburgh, U K

Beghin, C , and R Debrie (1972), Characteristics of the electric field far from and close to a radiating antenna around the lower hybrid resonance in the ionospheric plasma, *J Plasma Phys* , *8*, 287–310, doi 10 1017/S0022377800007157

Charbonneau-Lefort, M , B Afeyan, and M M Fejer (2008), Optical parametric amplifiers using chirped quasiphase-matching gratings I Practical design formulas, *J Opt Soc Am B*, *25*, 463–480

Cramer, N F (1975), Parametric excitation of ion-cyclotron waves, *Plasma Phys* , *17*, 967–972, doi 10 1088/0032-1028/17/11/011

Cramer, N F , and W N -C Sy (1979), Parametric decay of magnetoacoustic oscillations in a cylindrical plasma, *J Plasma Phys* , *22*, 549–562, doi 10 1017/S0022377800010308

Drell, S D , H M Foley, and M A Ruderman (1965), Drag and propulsion of large satellite in the ionosphere An Alfven propulsion engine in space, *J Geophys Res* , *70*, 3131–3145, doi 10 1029/JZ070i013p03131

Estes, R D (1988), Alfven waves from an electrodynamic tethered satellite system, *J Geophys Res* , *93*, 945–956, doi 10 1029/JA093iA02p00945

Fuji, H A , et al (2009), Sounding rocket experiment of bare electrodynamic tether system, *Acta Astronaut* , *64*(2–3), 313–324, doi 10 1016/j actaastro 2008 07 006

Gushchin, M , A Kostrov, S Korobkov, A Strikovsky, D Yanin, M Starodubtsev, V Gundorin, and A Mochalov (2006), Whistler wave experiments on large gKROTh device, *Rep 56*, Sodankyla Geophys Obs , Sodankyla, Finland

Hastings, D E , and J Wang (1987), The radiation impedance of an electrodynamic tether with end connectors, *Geophys Res Lett* , *14*, 519–522, doi 10 1029/GL014i005p00519

Hastings, D E , A Barnett, and S Olbert (1988), Radiation from large space structures in low Earth orbit with induced alternating current, *J Geophys Res* , *93*, 1945–1960, doi 10 1029/JA093iA03p01945

Hertzberg, M P , N F Cramer, and S V Vladimirov (2003), Parametric instabilities of Alfven waves in a dusty plasma, *Phys Plasmas*, *10*(8), 3160–3167, doi 10 1063/1 1591184

Hertzberg, M P , N F Cramer, and S V Vladimirov (2004), Parametric instabilities in a magnetized multicomponents plasmas, *Phys Rev E*, *69*, 056402, doi 10 1103/PhysRevE 69 056402

Inan, U S , T F Bell, J Bortnik, and J M Albert (2003), Controlled precipitation of radiation belt electrons, *J Geophys Res* , *108*(A5), 1186, doi 10 1029/2002JA009580

Janhunen, P (2004), Electric sail for spacecraft propulsion, *AIAA J Propulsion Power*, *20*(4), 763–764, doi 10 2514/1 8580

Janhunen, P , and A Sandroos (2007), Simulation study wind push on a charge wire Basis of solar wind electric sail propulsion, *Ann Geophys* , *25*, 755–767

Kaw, P K (1976), Parametric excitation of electromagnetic waves in magnetized plasmas, *Adv Plasma Phys* , *6*, 207–236

Korobkov, S V , M E Gushchin, A V Kostrov, A V Strikovskii, and C Krafft (2007), Near field of a loop antenna operating in plasma in the whistler frequency range, *Plasma Phys Rep* , *33*(2), 102–108, doi 10 1134/S1063780X07020031

Lehane, J A , and F J Paoloni (1972), Parametric excitation of Alfven waves, *Plasma Phys* , *14*, 461–471, doi 10 1088/0032-1028/14/5/004

Liu, C S , and P K Kaw (1976), Parametric instabilities in homogeneous unmagnetized plasmas, *Adv Plasma Phys* , *6*, 83–120

Liu, C S , M N Rosenbluth, and R B White (1973), Parametric scattering instabilities in inhomogeneous plasma, *Phys Rev Lett* , *31*, 697–700

Molchanov, O A , M M Mogilevsky, V V Afonin, Z Klos, M Hayakawa, and N Shima (1997), Nonlinear ELF-VLF effect observed on ACTIVNY satellite, in *Nonlinear Waves and Chaos in Space Plasmas*, edited by T Hada and H Matsumoto, pp 337–358, TERRAPUB, Tokyo

Nishikawa, K (1968), Parametric excitation of coupled waves I General formulation, *J Phys Soc Jpn* , *24*(4), 916–922, doi 10 1143/JPSJ 24 916

Perkins, F W , and J Flick (1971), Parametric instabilities in inhomogeneous plasmas, *Phys Fluids*, *14*(9), 2012–2018, doi 10 1063/1 1693711

Rosenbluth, M N (1972), Parametric instabilities in inhomogeneous media, *Phys Rev Lett* , *29*, 565–567

Sanmartin, J , and R Estes (1997), Alfvén wave far field from steady-current tethers, *J Geophys Res* , *102*, 14,625–14,630

Sanmartin, J , and M Martínez-Sánchez (1995), The radiation impedance of orbiting conductors, *J Geophys Res* , *100*, 1677–1686, doi 10 1029/94JA02857

Sanmartin, J R , M Charro, J Pelaez, I Tinao, S Elaskar, A Hilgers, and M Martinez-Sanchez (2006), Floating bare tether as upper atmosphere probe, *J Geophys Res* , *111*, A11310, doi 10 1029/2006JA011624

Short, R W , and A Simon (2004), Theory of three-wave parametric instabilities in inhomogeneous plasma revisited, *Phys Plasmas*, *11* (11), 5335–5340, doi 10 1063/1 1798451

Sonwalkar, V S , et al (2004), Diagnostics of magnetospheric electron density and irregularities at altitudes <5000 km using whistler and *Z* mode echoes from radio sounding on the IMAGE satellite, *J Geophys Res* , *109*, A11212, doi 10 1029/2004JA010471

Stark, J P W (2003), *Spacecraft Systems Engineering*, edited by P Fortescue, J Stark, and G Swinerd, John Wiley, New York

Vahala, G , and D Montgomery (1971), Parametric amplification of Alfvén waves, *Phys Fluids*, *14*(6), 1137–1140, doi 10 1063/1 1693576

G Sanchez-Arriaga and J R Sanmartin, Escuela Técnica Superior de Ingenieros Aeronáuticos, Universidad Politécnica de Madrid, Madrid E-28040, Spain (gonzalo sanchez@upm es)